Radiology

Intraoperative Supine Breast MR Imaging to Quantify Tumor Deformation and Detection of Residual Breast Cancer: Preliminary Results[1]

Eva C. Gombos, MD
Jagadeesan Jayender, PhD
Danielle M. Richman, MS, MD
Diana L. Caragacianu, MD
Melissa A. Mallory, MD
Ferenc A. Jolesz, MD†
Mehra Golshan, MD

Purpose: To use intraoperative supine magnetic resonance (MR) imaging to quantify breast tumor deformation and displacement secondary to the change in patient positioning from imaging (prone) to surgery (supine) and to evaluate residual tumor immediately after breast-conserving surgery (BCS).

Materials and Methods: Fifteen women gave informed written consent to participate in this prospective HIPAA-compliant, institutional review board–approved study between April 2012 and November 2014. Twelve patients underwent lumpectomy and postsurgical intraoperative supine MR imaging. Six of 12 patients underwent both pre- and postsurgical supine MR imaging. Geometric, structural, and heterogeneity metrics of the cancer and distances of the tumor from the nipple, chest wall, and skin were computed. Mean and standard deviations of the changes in volume, surface area, compactness, spherical disproportion, sphericity, and distances from key landmarks were computed from tumor models. Imaging duration was recorded.

Results: The mean differences in tumor deformation metrics between prone and supine imaging were as follows: volume, 23.8% (range, −30% to 103.95%); surface area, 6.5% (range, −13.24% to 63%); compactness, 16.2% (range, −23% to 47.3%); sphericity, 6.8% (range, −9.10% to 20.78%); and decrease in spherical disproportion, −11.3% (range, −60.81% to 76.95%). All tumors were closer to the chest wall on supine images than on prone images. No evidence of residual tumor was seen on MR images obtained after the procedures. Mean duration of pre- and postoperative supine MR imaging was 25 minutes (range, 18.4–31.6 minutes) and 19 minutes (range, 15.1–22.9 minutes), respectively.

Conclusion: Intraoperative supine breast MR imaging, when performed in conjunction with standard prone breast MR imaging, enables quantification of breast tumor deformation and displacement secondary to changes in patient positioning from standard imaging (prone) to surgery (supine) and may help clinicians evaluate for residual tumor immediately after BCS.

Online supplemental material is available for this article.

[1] From the Departments of Breast Imaging (E.C.G.), Radiology (J.J., D.M.R., F.A.J.), and Surgery (D.L.C., M.A.M., M.G.), Brigham and Women's Hospital, 75 Francis St, Boston, MA 02115. Received July 14, 2015; revision requested September 4; revision received March 10, 2016; accepted March 31; final version accepted April 15. **Address correspondence to** E.C.G. (e-mail: *egombos@partners.org*).

† Deceased.

Supported by the National Institutes of Health (R25 CA089017), National Center for Research Resources (P41EB015898), Breast Cancer Research Foundation, and the National Institute of Biomedical Imaging and Bioengineering (P41RR019703).

Breast-conserving therapy, which consists of lumpectomy followed by whole-breast irradiation, is a standard option used to treat early stage breast cancer. Positive margins increase the risk of local recurrence; therefore, clear margins are a prerequisite for breast-conserving therapy. In the United States, 20%–40% of patients undergoing breast-conserving surgery (BCS) require re-excision (1–7).

Contrast material–enhanced breast magnetic resonance (MR) imaging is an important modality used to detect malignancy, with reports of higher sensitivity than that attained with conventional imaging (sensitivity and specificity of approximately 90% and 85%, respectively) in the detection of breast cancer (8–11). However, there is no evidence that preoperative work-up with MR imaging for surgical planning or evaluation of disease extent translates into improved surgical outcome. Two prospective studies and a meta-analysis reported that patients undergoing preoperative MR imaging have not experienced reduced re-excision or improved survival rates (12–15). Critics of the existing studies performed to examine the value of preoperative breast MR imaging have highlighted the lack of a consistent strategy to manage MR imaging data (16,17). Additional findings were not always addressed and often did not generate specific modifications at the time of surgery. These inconsistencies may explain the lack of data supporting routine use of preoperative MR imaging in the evaluation of known breast carcinoma.

Our hypothesis is that intraoperative supine MR imaging can be used to plan the extent of resection, to detect residual tumor immediately after the first attempt at definitive surgery, and to provide feedback to the surgeon within the surgical suite. The aim of this study was to use intraoperative supine MR imaging to quantify breast tumor deformation and displacement secondary to the change in patient positioning from imaging (prone) to surgery (supine) and to evaluate the residual tumor immediately after BCS.

Advances in Knowledge

- We describe supine pre- and postprocedural MR imaging protocols and workflow within the operating room.
- The computed mean difference in tumor deformation metrics between supine and prone MR imaging examinations are as follows: *(a)* increases in volume, 23.8% (range, −30% to 103.95%); surface area, 6.5% (range, −13.24% to 63%); compactness, 16.2% (range, −23% to 47.3%); and sphericity, 6.8% (range, −9.10% to 20.78%) and *(b)* decrease in spherical disproportion, −11.3% (range, −60.81% to 76.95%).
- All tumors (n = 6) were closer to the chest wall on supine images than on prone images.
- The mean duration of pre- and postoperative supine MR examinations within the operating room was 25 minutes (range, 18.4–31.6 minutes) and 19 minutes (range, 15.1–22.9 minutes), respectively.

Materials and Methods

For this institutional review board–approved Health Insurance Portability and Accountability Act–compliant prospective trial, 15 patients provided written informed consent to participate in a phase I trial investigating the feasibility of intraoperative MR imaging for real-time margin analysis during BCS in the operating room imaging suite. At the 2014 annual meeting of the American Society of Breast Surgeons, we presented a video report on the feasibility of intraoperative MR imaging without further analysis in eight of the 15 patients (18).

MR imaging–guided BCS surgery was performed in an advanced multimodality image-guided operating suite (or AMIGO). This is an operating room and interventional suite with a full array of imaging modalities for use during procedures (18). There is a ceiling-mounted 3-T wide-bore (70 cm) MR imager (Verio; Siemens, Erlangen, Germany) in the center of the MR imaging room that can be moved in and out of the surgical field. The MR imager can traverse on rails to a fully draped patient on the operating table. The operating room is equipped with MR imaging conditional anesthesia delivery, monitoring systems, and instruments required to perform BCS (19). All images and information relevant to the procedure are accessible in the operating suite, with selected imaging series displayed on large liquid crystal display monitors within the room that

Implications for Patient Care

- Supine MR imaging may aid in improving surgical planning by accounting for tumor displacement and deformation occurring between standard positioning for MR imaging and that for surgery to potentially allow for more complete tumor resection.
- If validated in future large studies, intraoperative supine MR imaging could be expected to help detect a remnant tumor immediately after breast-conserving surgery to ensure negative surgical margins.

Published online before print
10.1148/radiol.2016151472 **Content codes:** BR MR

Radiology 2016; 281:720–729

Abbreviations:
BCS = breast-conserving surgery
HER2 = human epidermal growth factor receptor type 2
3D = three-dimensional
VIBE = volume-interpolated breath-hold examination

Author contributions:
Guarantors of integrity of entire study, E.C.G., F.A.J., M.G.; study concepts/study design or data acquisition or data analysis/interpretation, all authors; manuscript drafting or manuscript revision for important intellectual content, all authors; approval of final version of submitted manuscript, all authors; agrees to ensure any questions related to the work are appropriately resolved, all authors; literature research, E.C.G., J.J., D.L.C., M.G.; clinical studies, E.C.G., J.J., D.L.C., M.A.M., M.G.; statistical analysis, E.C.G., J.J.; and manuscript editing, all authors

Conflicts of interest are listed at the end of this article.

Table 1

MR Sequence Information for Diagnostic and Intraoperative Examinations

Sequence	Standard Diagnostic Breast MR Imaging	Preprocedure Breast MR Imaging	Postprocedure Supine Breast MR Imaging
Set-up	Prone, at a prior date	Supine, intraoperative	Supine, intraoperative
Imager and coil	3-T Magnetom Trio (Siemens Healthcare, Erlangen, Germany) and seven-channel breast surface coil (Invivo, Gainesville, Fla)	3-T Verio imager and 16-channel cardiac coil (IMRIS, Winnipeg, Canada)	3-T Siemens Verio imager and the aforementioned 16-channel cardiac coil
Sequences performed	Three-plane localizer; axial fat-suppressed T2-weighted fast spin-echo or T2-weighted short inversion time inversion recovery; axial fast spoiled gradient-echo T1-weighted non–fat-suppressed; unenhanced axial T1-weighted fat-suppressed three-dimensional (3D) fast spoiled gradient-echo (VIBE)*; contrast-enhanced† axial T1-weighted fat-suppressed 3D fast spoiled gradient-echo at around 90, 180, 270, and 360 seconds; and sagittal delayed T1-weighted fat-suppressed 3D fast spoiled gradient-echo	Three-plane localizer; axial fat-suppressed T2; unenhanced axial T1-weighted fat-suppressed 3D fast spoiled gradient-echo (VIBE)*; contrast-enhanced† axial T1-weighted fat-suppressed 3D fast spoiled gradient-echo at around 90, 180, 270, and 360 seconds; and sagittal delayed T1-weighted fat-suppressed 3D fast spoiled gradient-echo	Three-plane localizer; axial fat-suppressed T2; unenhanced axial T1-weighted fat-suppressed 3D fast spoiled gradient-echo (VIBE)*; contrast-enhanced† axial T1-weighted fat-suppressed 3D fast spoiled gradient-echo at around 130, 220, 310, and 400 seconds‡; and sagittal delayed T1-weighted fat-suppressed 3D fast spoiled gradient-echo
Sequence parameters	Repetition time msec/echo time msec, 4.4/1.76; 8° flip angle; 391 Hz/pixel bandwidth; 512 × 512 matrix; and 2-mm section thickness	4.93/1.8, 8° flip angle, 384 Hz/pixel bandwidth, 352 × 352 matrix, 2-mm section thickness	4.93/1.8, 8° flip angle, 384 Hz/pixel bandwidth, 352 × 352 matrix, 2-mm section thickness
Postprocessing	Subtraction axial images, maximum intensity projection, and computer-aided diagnosis	Subtraction axial images, maximum intensity projection, and computer-aided diagnosis	Subtraction axial images, maximum intensity projection, and computer-aided diagnosis

* Intraoperative volume-interpolated breath-hold examination (VIBE) sequences were performed during a controlled breath hold, with patient anesthesia suspended by the anesthesiology team. Because the chest wall movements are more pronounced in the supine position than in the prone position, breath-hold imaging aids in avoiding motion artifacts that degrade image quality and cause misregistration on subtraction images.

† Intravenous administration of 0.1 mmol/kg gadopentetate dimeglumine (Magnevist; Bayer Healthcare, Wayne, NJ).

‡ During postprocedural MR imaging, additional delay times were added to account for the assumed reduced perfusion immediately after surgery. With the surgical insult, swelling to the parenchyma with tissue edema occurring increased when saline filled the cavity. We expected that enhancement on the postlumpectomy MR images would be reduced and that the signal peak would be delayed.

enable surgeons to continuously view relevant imaging data.

Participants and MR Imaging Sequences

The operating breast surgical oncologist (M.G.) recruited the subjects. Eligible patients were women aged 18–74 years with core biopsy–proved clinical stage I or II invasive breast cancer who had MR imaging–measurable disease and who were candidates for BCS. Exclusion criteria were prior ipsilateral breast cancer or breast surgery, any prior breast reconstruction or implants, current neoadjuvant therapy or enrollment in other preoperative trials, pregnancy or breast feeding, and hereditary predisposition to breast cancer, such as *BRCA* mutations, Li-Fraumeni syndrome, or Cowden disease.

Between April 2012 and December 2014, a total of 15 women were enrolled. Two patients had extensive breast cancer and were not considered suitable for the procedure. A third patient with a separate comorbidity of lung cancer as an additional primary cancer was also excluded.

Each patient underwent standard diagnostic MR imaging in the usual prone position as an outpatient prior to surgery. The details of the imaging sequences are shown in Table 1. The surgeon (M.G.) and procedure radiologist (E.C.G.) reviewed available additional breast imaging studies, including mammograms, sonograms, and core biopsy samples. Six of the first seven patients underwent preprocedural MR imaging in the operating room, and all 12 patients underwent postprocedural intraoperative breast MR imaging after removal of the main tumor. One of the first seven patients did not undergo preprocedure MR imaging due to time constraints. This patient also had undergone preoperative contrast material–enhanced MR imaging–guided wire localization, which was another reason we chose not to perform additional intraoperative MR imaging. An example of timing of sequences is shown in Table 2.

Although preprocedure supine MR imaging yielded high-spatial-resolution images, it was excessively time consuming; therefore, we suspended preprocedure supine MR imaging at the time of surgery after we processed the first seven studies.

Personnel

Procedures were performed by a breast radiologist with 11 years of experience in breast MR image interpretation (E.C.G.), two MR technologists, a breast surgical oncologist (M.G.), and two surgical fellows (D.L.C., M.A.M.). In addition, an imaging scientist (J.J.),

Table 2

Example of Calculated Dynamic Series Acquisition Timings and Breath-hold Times of Pre- and Postprocedural MR Imaging Examinations

Step in Preprocedural MR Imaging	Time (sec)	Step in Postprocedural MR Imaging	Time (sec)
…	…	Time to prepare the patient for imaging after surgery (ie, cover the operative field, adjust drapes)	540
…	…	Safety check prior to the MR imaged entering the room	160
Imager moves over the patient into the room	90	Imager moves over the patient into the room	90
Unenhanced axial VIBE breath-hold sequence imaging time	24	Unenhanced axial VIBE breath-hold sequence imaging time	27
Contrast material injection starts		Contrast material injection starts	
Ventilation by anesthesiologist. Wait 120 seconds minus the imaging time	96	Ventilation by anesthesiologist. Wait 130 seconds minus the imaging time.	103
15 seconds before end of wait time start breath hold at	81	15 seconds before end of wait time start breath hold at	88
Contrast-enhanced first axial VIBE runtime in breath hold	24	Contrast-enhanced first axial VIBE runtime in breath hold	27
Ventilation by anesthesiologist. Wait 90 seconds minus imaging time	66	Ventilation by anesthesiologist. Wait 90 seconds minus imaging time	63
15 seconds before end of wait time start breath hold at	51	15 seconds before end of wait time start breath hold at	48
Contrast-enhanced second axial VIBE runtime in breath hold	24	Contrast-enhanced second axial VIBE runtime in breath hold	27
Ventilation by anesthesiologist. Wait 90 seconds minus imaging time	66	Ventilation by anesthesiologist. Wait 90 seconds minus imaging time	63
15 seconds before end of wait time start breath hold at	51	15 seconds before end of wait time start breath hold at	48
Contrast-enhanced third axial VIBE runtime in breath hold	24	Contrast-enhanced third axial VIBE runtime in breath hold	27
Ventilation by anesthesiologist. Wait 90 seconds minus imaging time	66	Ventilation by anesthesiologist. Wait 90 seconds minus imaging time	63
15 seconds before end of wait time start breath hold at	51	15 seconds before end of wait time start breath hold at	48
Contrast-enhanced fourth axial VIBE runtime in breath hold	24	Contrast-enhanced fourth axial VIBE runtime in breath hold	27
Ventilation by anesthesiologist. Wait 90 seconds minus imaging time	66	Ventilation by anesthesiologist. Wait 90 seconds minus imaging time	63
15 seconds before end of wait time start breath hold at	51	15 seconds before end of wait time start breath hold at	48
Contrast-enhanced sagittal T1 imaging (performed right after last axial examination)	90	Contrast-enhanced sagittal T1 imaging (performed right after last axial examination)	90
Imager moves away from its position over the patient and out of the room	90	Imager moves away from its position over the patient and out of the room	90

Note.—The anesthesiologist suspends ventilation during the examination, resulting in a controlled breath hold. This is only an example, and times varied between patients.

the chief nurse in-charge, anesthesiologists, and administrative personnel were involved and present during the procedures.

Imaging Surgery Workflow

Prior to live procedures, multiple dry-run tests with volunteers were performed to develop and study the optimal workflow (Fig 1, Fig E1 [online]). The information gleaned from these experiments helped us define the workflow for the BCS procedures and subsequently enabled us to decrease time in the operating room.

On the day of the surgery, the patient was placed in the supine surgical position, and general anesthesia was introduced. Six of the patients underwent preprocedural supine MR imaging prior to BCS in the operating room. For supine sequences, the patient was carefully positioned to achieve adequate breast tissue visualization and to minimize skin folds and other artifacts to optimize image quality. The patient's shoulders were propped up with cushions to allow the breast to rest medially. The lower part of a 16-channel cardiac coil was placed in an empty cartridge without moving the patient, and the upper coil was gently placed over the operative breast with a sterile cover without applying additional pressure on the breast. After we completed a rigorous checklist to ensure that all ferrous materials, equipment, and booms were moved beyond the 0.0005-T line, the ceiling-mounted MR imager traversed over the patient to perform preprocedural MR imaging.

On completion of preprocedural imaging, the MR imager was moved out of the operating room. The patient then underwent standard sentinel lymph node biopsy and lumpectomy with or without preoperative wire localization. After BCS, the lumpectomy cavity was filled with normal saline to match the resected volume calculated with diagnostic MR imaging. An earlier work showed magnetic susceptibility mismatch of the air-tissue interface created a high-signal-intensity artifact that could be mistaken for enhancement (20). As the susceptibility of saline approximately matches that of tissue, filling the cavity with saline before postsurgical imaging can help minimize the artifact. The lumpectomy cavity was temporarily closed with sutures, and the surgical region was covered with sterile dressing to maintain sterility. The removed specimen was transferred for routine specimen radiography to document target removal and wire integrity. The patient

Figure 1

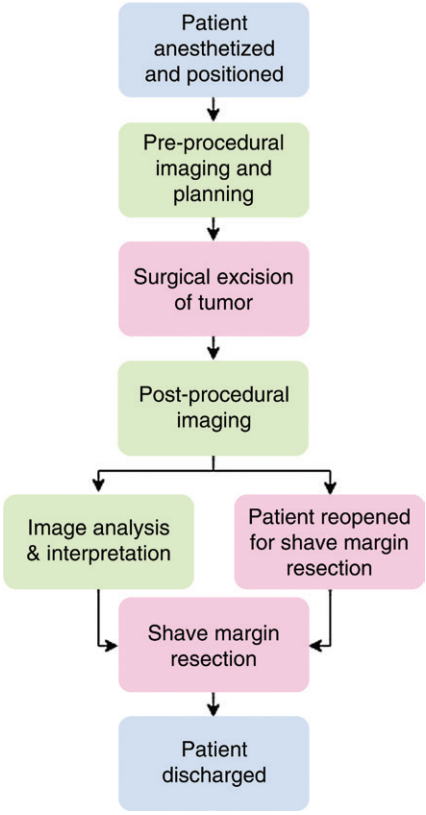

Figure 1: Flowchart shows imaging workflow on the day of surgery in the operating room imaging suite. All patients underwent standard diagnostic dynamic contrast-enhanced breast MR imaging in the prone position on a prior day. Image-guided wire localization, if necessary, was performed prior to surgery with MR imaging–conditional wire.

was then undraped and prepared for postprocedural MR imaging.

Immediately after surgery, the patient was imaged in the sterile surgical area with a similar careful positioning and coil set-up as with the supine MR imaging performed prior to surgery. Skin markers (MR-SPOTS; Beekley Medical, Bristol, Conn) were placed inferior and superior to the surgical cavity to aid in planning the imaging volume on the localizer images. The radiologist provided a detailed report on suspicious enhancement and possible remnant tumor to the surgeon. The radiologist and surgeon discussed the images, and the surgeon indicated clinically suspicious areas. The surgeon then performed shave resection at six standard cavity margins in which a thin fragment of additional tissue was resected at the anterior, posterior, medial, lateral, and superior margins.

Contrast Material Administration

Gadopentetate dimeglumine at a concentration of 0.1 mmol per kilogram of body weight (0.2 mL per kilogram of body weight) with a maximum dose of 15 mL was administered in the intraoperative setting on the same day as the procedure. Six patients who underwent both pre- and postprocedure MR imaging received two injections of intraoperative intravenous MR contrast material. The dose for two intraoperative MR examinations did not exceed 30 mL. Our protocol adhered to Food and Drug Administration guidelines for routine intravenous injection of a 0.15 mmol/kg (0.3 mL/kg) gadolinium-containing contrast material, with a maximum safe dose of 30 mL. A question remained, however, as to image quality and contrast resolution, as the two injections of the gadolinium chelate were administered within a short interval (approximately 1.5–2.0 hours apart). We expected that the second intraoperative MR imaging precontrast VIBE sequence would depict low baseline tissue intensity without detectable contrast enhancement and that the contrast-enhanced MR images would be adequate to show enhancement. Although there is no quantitative measure of image adequacy, the radiologist qualitatively assessed each case as satisfactory or unsatisfactory for resolution, tissue contrast, and delivery of intravenous contrast material.

Procedure Planning

On the basis of the patient's diagnostic planning MR images obtained prior to the surgical procedure, the radiology team (J.J., E.C.G.), prepared detailed 3D schemes for the surgeon. The tumor was segmented on MR images by using CADstream software (Merge Healthcare, Chicago, Ill). The Digital Imaging and Communications in Medicine volume of the diagnostic MR imaging study was loaded into the open-source software (3D Slicer; *https://www.slicer.org/slicerWiki/index.php/Main_Page*). The first contrast-enhanced MR imaging study was volume rendered with increased transparency of the breast to depict the 3D structure of the tumor. The volume of the surgical cavity, assuming a 10-mm margin around the tumor, was computed to determine the amount of saline to be injected into the cavity immediately after the procedure.

Pre- and Postprocedural Image Analysis

Pre- and postprocedural MR images were provided intraoperatively to the CADstream software to automatically segment the tumor corresponding to the regions of enhancement presumed to be due to angiogenesis. Subtracted images, which were computed from the first and fourth unenhanced and contrast-enhanced images, were computed and provided to the radiologist for analysis. This processing was performed when the MR imager was being moved out of the operating room and while the patient was being prepared after both intraoperative pre- and postprocedural MR studies.

Duration of Intraoperative MR Imaging

We documented the elapsed time between acquisition of the first and last images for pre- and postoperative examinations. The recorded duration shows total MR image acquisition times. It does not include the time taken to prepare the surgical site, position the coil on the patient, or move the imager. (Each time the imager moves, it takes approximately 90 seconds.)

Imaging Processing, Computer-aided Diagnosis, and Deformation Mapping

Postprocessing, including axial subtraction images, maximum intensity projection images, and computer-aided detection analysis, was performed routinely at all stages of breast MR imaging and was used in the diagnostic work-up and for intraoperative decision making.

We investigated the effect of a change in patient position (ie, from prone in the diagnostic phase to supine in the surgical phase) on tumor deformation and displacement, based on

segmentation of the tumor performed by the radiology team. Initially, after we aligned the pulmonary veins, contrast-enhanced images in the prone and supine positions were rigidly registered based on thoracic cavities by using the mutual information criterion (21–23). Then, 3D tumor models were created with the aforementioned 3D Slicer software by segmenting the tumors on supine and prone MR images with semiautomatic threshold-based algorithms on the subtraction images computed from the first unenhanced and contrast-enhanced volumes (23). The 3D models were further registered by using iterative closest point registration. We used the HeterogeneityCAD module in the 3D Slicer software *(https://www.slicer.org/slicerWiki/index.php/Documentation/Nightly/Modules/HeterogeneityCAD)* to compute 65 geometric, structural, and heterogeneity metrics, including volume, surface area, maximum 3D diameter, compactness, spherical disproportion, and sphericity for the tumors segmented on prone and supine MR images. Distances of the tumor center from the nipple, chest wall, and skin were computed. Care was taken regarding tumors close to the chest wall to ensure accurate delineation of the tumor to plan the extent of surgery.

Statistical Methods

The Student *t* test was performed to evaluate whether there was a significant difference ($P < .05$) between the intraprocedural imaging time change for the first three patients and the second three patients. We used the univariate Mann-Whitney test to compare supine and prone MR imaging tumor deformation and displacement metrics. Statistical analyses were performed by using MATLAB software (MathWorks; Natick, Mass).

Results

No technical or procedural complications were encountered when obtaining postprocedural MR images. Subjective assessment showed no susceptibility artifacts at the air-tissue boundary, and postprocedure saline-infused images were determined to be satisfactory and of high spatial resolution (Fig E2 [online]).

Clinical and imaging data in the six women who underwent both pre- and postlumpectomy intraoperative MR imaging are summarized in Table 3. The average greatest MR imaging dimension of the cancers was 2.0 cm (range, 1.4–3.0 cm) on diagnostic prone MR images. Mean tumor volume was 1.66 cm^3 (range, 0.13–3.6 cm^3) per MR image. The mean cavity volume was 31.98 cm^3 (range, 13.7–54.0 cm^3), as measured on postprocedural MR images.

Tumor Deformation Due to Position Change

We found deformation and displacement of the tumor in the six patients in whom we obtained prone diagnostic and supine preprocedural MR images (Fig 2; Figs E2, E3 [online]). The mean change from prone images to supine images (as a percentage of the prone metrics) was as follows: *(a)* increase in volume, 23.8% (range, −30%, 103.95%); surface area, 6.5% (range, −13.24% to 63%); compactness, 16.2% (range, −23% to 47.3%); spherical disproportion −11.3% (range, −60.81% to 76.95%); and sphericity, 6.8% (range, −9.10% to 20.78%) and *(b)* decrease in spherical disproportion, −11.3% (range, −60.81% to 76.95%) (Table 4). No significant differences were observed between metrics for the supine or prone positions. For the six patients analyzed, the average tumor displacement was 23.8, −27.7, and −6.5 mm in the lateral, anterior, and superior coordinates, respectively. All the tumors were closer to the chest wall on supine images than on prone images.

Comparison with Histopathology Results

The final histopathology results were similar to those for histopathology of the core biopsy. However, in two patients, histopathology of the excision specimen showed higher grades of invasive cancer. In addition, in three patients, histopathology of the lumpectomy specimen revealed that ductal carcinoma in situ was present around the invasive cancers, all of which were without an extensive intraductal component.

The mean largest dimension of the cancers measured on diagnostic prone MR images was 2.0 cm (range, 1.4–3.0 cm). In two patients, benign pattern of enhancement was seen on postprocedural MR images (a focus and nonmasslike enhancement); however, these were not suspicious for residual tumor.

The mean of largest dimension of the cancers measured at final pathologic examination was 2.0 cm (range, 1.6–2.7 cm) (Table 3). One patient underwent re-excision in a different session because of histopathologic findings, revealing a 2-mm area of ductal carcinoma in situ at pathology. This was not seen on postprocedure MR images.

Duration of Intraoperative Imaging

The mean duration of the preoperative supine examination was 25 minutes ± 6.6 (standard deviation) (range, 17.7–37 minutes). The mean duration of the postlumpectomy supine examination was 19 minutes ± 3.9 (range, 13.1–25.9 minutes). The MR imaging time did not decrease with team experience during the 14 months of this study (Table 3). The first three and second three examinations lasted an average of 26 and 24 minutes, respectively, preoperatively ($P = .59$) and an average of 18 and 21 minutes, respectively, postoperatively ($P = .41$).

Discussion

MR imaging confers a high level of sensitivity in breast tumor detection, and it has often been used to image residual tumors after lumpectomy. Studies in patients with positive or close tumor margins who are undergoing MR imaging before re-excision showed that MR imaging is able to depict residual disease, with false-positive results caused by inflammatory processes that resemble residual disease (24,25). Soderstrom et al reported MR imaging has an accuracy of approximately 84% in the detection of recurrent tumors in patients who have recently undergone BCS (26). Posttherapeutic effects may cause substantial enhancement within the treated breast, primarily within the first 12 months after

Table 3

Patient Demographics, MR Imaging, Pathology Findings, and Pre- and Postoperative MR Imaging Times in the Six Patients with Both Pre- and Postoperative Supine MR Imaging in the Operating Room Imaging Suite

Characteristic	Patient 1	Patient 2	Patient 3	Patient 4*	Patient 5	Patient 6
Age (y)	54	59	53	43	64	34
Side involved	Right	Right	Right	Right	Left	Right
Quadrant	Lower outer	Upper (12 o'clock)	Upper outer	Upper inner	Upper outer	Upper inner
Breast density	Scattered fibroglandular	Heterogeneously dense	Heterogeneously dense	Scattered fibroglandular	Extremely dense	Extremely dense
Multifocal per MR imaging	No	No	No	No	No	No
Other imaging findings	None	None	None	Additional foci of enhancement with washout medially, anteriorly and posteriorly to the dominant mass	None	None
Size on prone MR images (cm)	3.0 × 1.6 × 2.0	2.0 × 1.6 × 1.5	1.4 × 1.0 × 1.0	2 × 1.8 × 1.5	2 × 1.8 × 1.5	1.4 × 1.2 × 1.0
Dynamic contrast-enhanced MR imaging enhancement	Heterogeneous with rapid rise, washout	Heterogeneous with rapid rise, washout	Heterogeneous with rapid rise, plateau	Heterogeneous with rapid rise, washout	Heterogeneous with rapid rise, washout	Heterogeneous with rapid rise, washout
Tumor volume (cm^3)	3.6	2.6	0.13	1.8	1.3	0.55
Cavity volume = tumor + 1.0 cm margin (cm^3)	54	41.1	13.7	38.1	27.3	17.7
Postprocedure imaging findings	No enhancement	No enhancement	No enhancement	Foci of rapid enhancement in the lateral and medial upper inner quadrant	5-mm enhancing focus superiorly anteriorly to the cavity	No enhancement
Preoperative path	ILC, Grade 2	IDC, Grade 2	IDC, Grade 1	Mixed ductal and lobular invasive cancer, G1 and DCIS	IDC, Grade 2	IDC, Grade 2
Postopearative (final) pathology	ILC, Grade 2	IDC, Grade 2	IDC, Grade 2	Mixed ductal and lobular invasive cancer, Grade 1	IDC, Grade 3	IDC, Grade 2
Ductal carcinoma in situ present	No	Yes	No	Yes	Yes	No
Receptor status	ER positive, PR positive, HER2/*neu* negative	ER positive, PR positive, HER2/*neu* equivocal	ER positive, PR positive, HER2/*neu* positive	ER positive, PR , positive, HER2/*neu* negative	ER positive, PR negative, HER2/*neu* negative	ER positive, PR positive, HER2/*neu* negative
Excisional specimen margin status	Close superior, others negative	Negative	Close anterior, others negative.	Very close for DCIS superior, medial, and lateral; others negative	Negative	Very close for posterior and superior; close all others negative
Final (shave) margin for invasive cancer	Negative	Negative	Negative	Negative*	Negative	Negative
Lymph nodes	Negative	Negative	Negative	Negative	Negative	Negative
Pathology size (cm)	2.5	2.0 × 1.7 × 1.6	1.4 × 0.9	2.0 × 1.3 × 1.2	2.7 × 1.8 × 1.6	1.6 × 1.2 × 1.0
Preoperative imaging time (min)	17.7	37	24.9	27	23	21.1
Postoperative imaging time (min)	21.1	13.1	20	25.9	18.1	17.8

Note.—Pathology type and grade: IDC = invasive ductal carcinoma, ILC = invasive lobular carcinoma. Grade 1, well-differentiated invasive cancer; grade 2, moderately differentiated invasive cancer; grade 3, poorly differentiated invasive cancer. Pathology margin status: negative, inked margin is more than 0.3 cm from carcinoma; close, inked margin is 0.1–0.3 cm from carcinoma; very close, inked margin is less than 0.1 cm from carcinoma. Positive, ink on carcinoma. ER = estrogen receptor, HER2 = human epidermal growth factor receptor 2, PR = progesterone receptor.

* One patient had a second operation at a different session, with pathologic analysis of the re-excision sample revealing residual ductal carcinoma in situ at the superior margin.

Figure 2

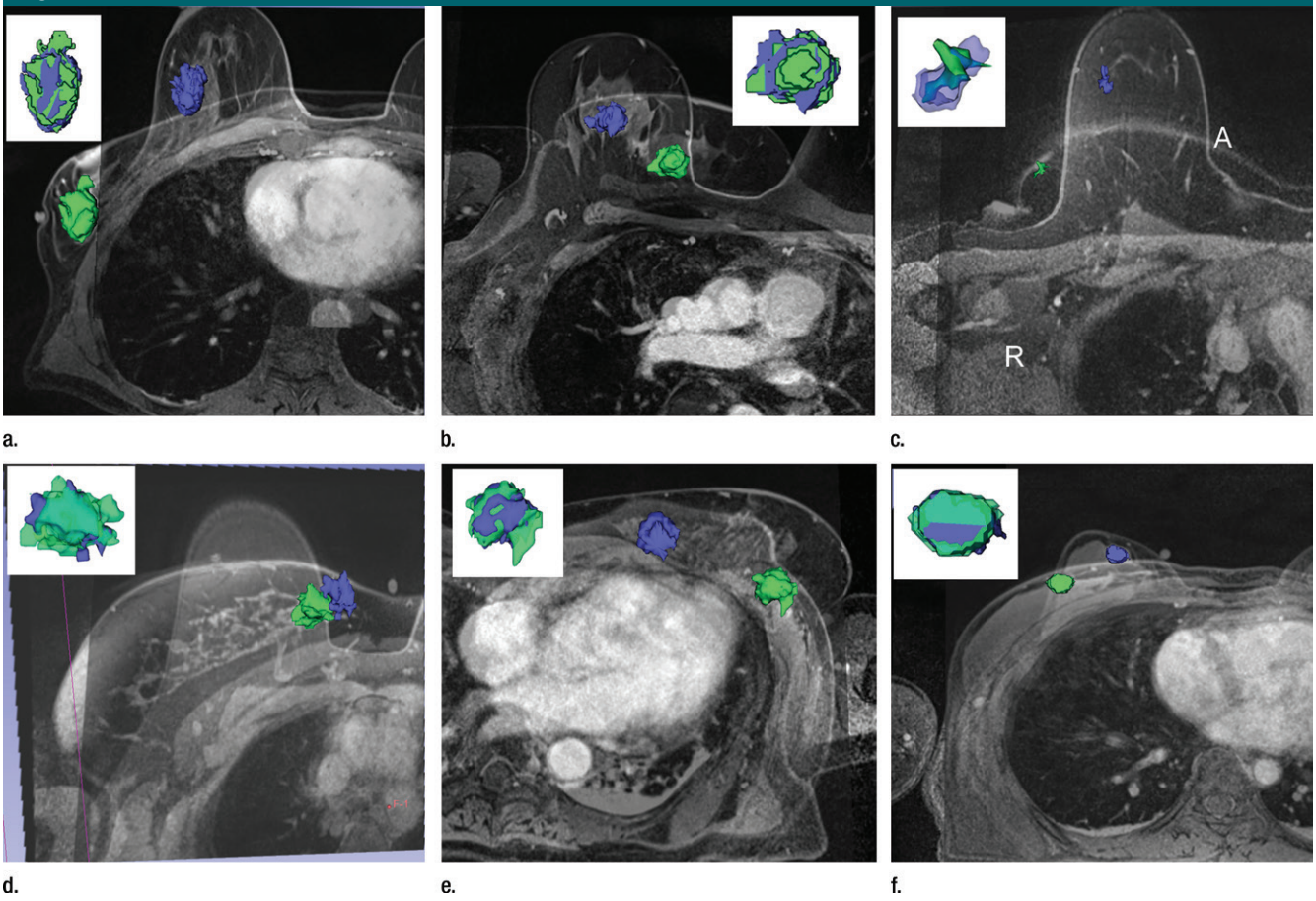

Figure 2: Breast and tumor deformation and displacement in six patients. Prone diagnostic and supine preprocedural contrast-enhanced MR images are superimposed on one another with 3D prone (blue) and supine (green) tumor models after iterative closest point registration. The surgeon can view these images intraoperatively to plan the surgical incision. **(a)** Images in a 52-year-old patient with moderately differentiated estrogen receptor, progesterone receptor–positive, and HER2/*neu*-negative invasive lobular cancer. **(b)** Images in a 59-year-old patient with moderately differentiated estrogen receptor, progesterone receptor–positive, and HER2/*neu*-equivocal invasive ductal cancer and ductal carcinoma in situ. **(c)** Images in a 53-year-old patient with moderately differentiated estrogen receptor, progesterone receptor–positive, and HER2/*neu*-positive invasive ductal cancer. **(d)** Images in a 43-year-old patient with a well-differentiated estrogen receptor, progesterone receptor–positive, and HER2/*neu*-positive mixed ductal and lobular cancer and ductal carcinoma in situ. **(e)** Images in a 64-year-old patient with poorly differentiated estrogen receptor, progesterone receptor–positive, and HER2/*neu*-positive invasive ductal cancer and ductal carcinoma in situ. **(f)** Images in a 34-year-old patient with moderately differentiated estrogen receptor, progesterone receptor–positive, and HER2/*neu*-positive invasive ductal cancer.

BCS; however, recurrent or residual carcinomas after BCS show rapid enhancement, which is typical of a malignant tumor (27). Krämer et al showed that MR imaging has the highest sensitivity (91%) in the detection of recurrent or residual tumor when compared with US (85%) or mammography (67%) (28). In an editorial, Jacobs concluded that in addition to improvements in surgical techniques, it is important to accurately assess surgical margins intraoperatively to prevent patients from returning for a second or third procedure at the current rate (one in five patients) (29).

In previous studies on the utility of MR imaging in the evaluation of the extent of cancer, the MR imaging findings were not systematically addressed, and the issues of tumor deformation and displacement were not investigated (15,16). The advanced multimodality image-guided operating (or AMIGO) suite enables intraoperative imaging with a state-of-the-art 3-T MR imager after addressing these issues. The success of a lumpectomy feasibility study with intraoperative MR imaging with a 0.5-T open imager and maintenance of sterility (20) was confirmed in a phase I clinical trial performed in the AMIGO suite with a 3-T imager (18). In this study, we showed that considerable deformity of the breast and tumor position occurs in the supine position.

The detected tumor displacement with a change in position was expected. The tumor deformation with position change was somewhat less anticipated.

Table 4

Changes in MR Imaging–associated Breast Tumor Heterogeneity Metrics Calculated as Supine Metric Minus Prone Metric in the Six Patients Who Underwent Both Pre- and Postprocedural Intraoperative Breast MR Imaging

Tumor Metric	Patient 1	Patient 2	Patient 3	Patient 4	Patient 5	Patient 6	Mean*
Volume (%)	58.6	−3.7	−30.0	104.0	−10.9	25.1	23.8 ± 49.9
Surface area (%)	12.6	−9.8	−13.2	63.0	−11.6	−1.4	6.5 ± 29.2
Maximum 3D diameter (%)	14.6	−1.7	−20.0	17.2	−0.5	−52.1	−7.1 ± 25.7
Surface-to-volume ratio (%)	−29.0	−6.4	23.9	−20.1	−0.8	−21.2	−8.9 ± 19.1
Compactness (%)	46.6	3.2	−23.0	47.3	−3.3	26.3	16.2 ± 28.5
Spherical disproportion (%)	−55.2	−2.8	77.0	−60.8	11.3	−37.0	−11.3 ± 51.8
Sphericity (%)	20.8	8.2	−9.1	−1.3	4.7	17.8	6.8 ± 11.3
Distance to chest wall (mm)	−13.5	−37.6	−28.7	−23.3	−6.1	−16.7	−20.97 ± 11.3
Distance to nipple (mm)	−21.3	−3.3	NA	4.1	−28.3	−10.2	−11.8 ± 13.1
Distance to skin (mm)	0.7	−5.9	3.6	3.4	1.4	−0.1	0.5 ± 3.8
Hausdorff distance (mm)	8.3	4.7	3.0	8.2	6.9	2.5	5.6 ± 2.6
Position difference (mm)							
Lateral	58.5	−34.0	36.2	0.3	51.4	30.5	23.8 ± 34.9
Anterior	−66.5	−24.5	−45.0	−1.5	−11.5	−17.0	−27.7 ± 24
Superior	7.7	−1.6	−24.3	50.5	−64.1	−7.3	−6.5 ± 37.7
Angulation difference (degrees)							
Lateral	14.8	−11.1	32.6	−58.8	16.1	63.9	9.6 ± 41.6
Anterior	−7.6	3.1	125.4	22.6	27.8	88.7	43.3 ± 52.3
Superior	−1.1	13.2	48.6	−55.9	43.5	119.0	27.9 ± 58.4

Note.—NA = not applicable.

* Data are mean ± standard deviaton.

Cancers are stiffer than the surrounding breast parenchyma; therefore, deformations of the tumor would be expected to be negligible. Krouskop et al showed that the stiffness of normal fat, normal glandular tissue, and invasive ductal carcinomas were 20, 57, and 490 kPa, respectively (30). Despite the difference in stiffness between the tumor and the surrounding breast parenchyma, we observed an average change of 23.8% in the measured volume, 6.5% in the surface area, 16.2% in compactness, and 7.1% in maximum 3D diameter.

Our study had limitations. We describe initial results in a small number of patients. We did not assess for errors or interobserver variability related to segmentation of the tumor on supine and prone dynamic contrast-enhanced MR images. In addition, the cost of using intraoperative MR imaging was not assessed. The practical applications are limited to the few sites (academic centers) that have the ability to perform this type of imaging. Although preoperative supine MR imaging yielded good quality high-spatial-resolution images, it was found to be too time consuming for practical use. Thus, preoperative supine MR imaging at the time of surgery was suspended after the first seven patients were examined. Instead, we are currently performing one imaging sequence with the patient in the supine position at the time of diagnostic prone MR imaging, and we do not perform a complete intraoperative examination in the supine position within the operating room.

In summary, we describe our experience with a supine MR imaging protocol and workflow. Tumor deformation and position were substantially different in the prone and supine studies. We hypothesize that supine MR imaging may assist in achieving more accurate tumor delineation and may enable more detailed surgical planning for lumpectomy procedures. Larger studies are needed for more thorough assessment.

Acknowledgment: We thank Nina Geller, PhD, for her valuable contribution in the preparation of this manuscript.

Disclosures of Conflicts of Interest: E.C.G. Activities related to the present article: disclosed no relevant relationships. Activities not related to the present article: received royalties from Amirsys Publishing. Other relationships: disclosed no relevant relationships. **J.J.** Activities related to the present article: disclosed no relevant relationships. Activities not related to the present article: received grants from Siemens and Symbow Medical; has multiple patents pending. Other relationships: disclosed no relevant relationships. **D.M.R.** disclosed no relevant relationships. **D.L.C.** disclosed no relevant relationships. **M.A.M.** disclosed no relevant relationships. **F.A.J.** disclosed no relevant relationships. **M.G.** disclosed no relevant relationships.

References

1. Camp ER, McAuliffe PF, Gilroy JS, et al. Minimizing local recurrence after breast conserving therapy using intraoperative shaved margins to determine pathologic tumor clearance. J Am Coll Surg 2005;201(6):855–861.

2. Cowen D, Houvenaeghel G, Bardou V, et al. Local and distant failures after limited surgery with positive margins and radiotherapy for node-negative breast cancer. Int J Radiat Oncol Biol Phys 2000;47(2):305–312.

3. Menes TS, Tartter PI, Bleiweiss I, Godbold JH, Estabrook A, Smith SR. The consequence of multiple re-excisions to obtain clear lumpectomy margins in breast cancer patients. Ann Surg Oncol 2005;12(11):881–885.

4. Russo AL, Arvold ND, Niemierko A, et al. Margin status and the risk of local recurrence in patients with early-stage breast cancer treated with breast-conserving therapy. Breast Cancer Res Treat 2013;140(2):353–361.

5. Sabel MS, Rogers K, Griffith K, et al. Residual disease after re-excision lumpectomy for close margins. J Surg Oncol 2009;99(2):99–103.

6. Smitt MC, Nowels KW, Zdeblick MJ, et al. The importance of the lumpectomy surgical margin status in long-term results of breast conservation. Cancer 1995;76(2):259–267.

7. Waljee JF, Hu ES, Newman LA, Alderman AK. Predictors of re-excision among women undergoing breast-conserving surgery for cancer. Ann Surg Oncol 2008;15(5):1297–1303.

8. Berg WA, Gutierrez L, NessAiver MS, et al. Diagnostic accuracy of mammography, clinical examination, US, and MR imaging in preoperative assessment of breast cancer. Radiology 2004;233(3):830–849.

9. Houssami N, Ciatto S, Macaskill P, et al. Accuracy and surgical impact of magnetic resonance imaging in breast cancer staging: systematic review and meta-analysis in detection of multifocal and multicentric cancer. J Clin Oncol 2008;26(19):3248–3258.

10. Medeiros LR, Duarte CS, Rosa DD, et al. Accuracy of magnetic resonance in suspicious breast lesions: a systematic quantitative review and meta-analysis. Breast Cancer Res Treat 2011;126(2):273–285.

11. Bluemke DA, Gatsonis CA, Chen MH, et al. Magnetic resonance imaging of the breast prior to biopsy. JAMA 2004;292(22):2735–2742.

12. Bilimoria KY, Cambic A, Hansen NM, Bethke KP. Evaluating the impact of preoperative breast magnetic resonance imaging on the surgical management of newly diagnosed breast cancers. Arch Surg 2007;142(5):441–445; discussion 445–447.

13. Houssami N, Turner R, Macaskill P, et al. An individual person data meta-analysis of preoperative magnetic resonance imaging and breast cancer recurrence. J Clin Oncol 2014;32(5):392–401.

14. Solin LJ, Orel SG, Hwang WT, Harris EE, Schnall MD. Relationship of breast magnetic resonance imaging to outcome after breast-conservation treatment with radiation for women with early-stage invasive breast carcinoma or ductal carcinoma in situ. J Clin Oncol 2008;26(3):386–391.

15. Turnbull L, Brown S, Harvey I, et al. Comparative effectiveness of MRI in breast cancer (COMICE) trial: a randomised controlled trial. Lancet 2010;375(9714):563–571.

16. Morris EA. Should we dispense with preoperative breast MRI? Lancet 2010;375(9714):528–530.

17. Sung JS, Li J, Da Costa G, et al. Preoperative breast MRI for early-stage breast cancer: effect on surgical and long-term outcomes. AJR Am J Roentgenol 2014;202(6):1376–1382.

18. Golshan M, Sagara Y, Wexelman B, et al. Pilot study to evaluate feasibility of image-guided breast-conserving therapy in the advanced multimodal image-guided operating (AMIGO) suite. Ann Surg Oncol 2014;21(10):3356–3357.

19. Tempany CM, Jayender J, Kapur T, et al. Multimodal imaging for improved diagnosis and treatment of cancers. Cancer 2015;121(6):817–827.

20. Hirose M, Kacher DF, Smith DN, Kaelin CM, Jolesz FA. Feasibility of MR imaging-guided breast lumpectomy for malignant tumors in a 0.5-T open-configuration MR imaging system. Acad Radiol 2002;9(8):933–941.

21. Johnson H, Harris G, Williams K. BRAINSFit: mutual information rigid registrations of whole-brain 3D images, using the insight toolkit. Insight J 2007; 1–10.

22. Viola P, Wells WM III. Alignment by maximization of mutual information. Int J Comput Vis 1997;24(2):137–154.

23. Fedorov A, Beichel R, Kalpathy-Cramer J, et al. 3D Slicer as an image computing platform for the Quantitative Imaging Network. Magn Reson Imaging 2012;30(9):1323–1341.

24. Stucky CC, McLaughlin SA, Dueck AC, et al. Does magnetic resonance imaging accurately predict residual disease in breast cancer? Am J Surg 2009;198(4):547–552.

25. Lee JM, Orel SG, Czerniecki BJ, Solin LJ, Schnall MD. MRI before reexcision surgery in patients with breast cancer. AJR Am J Roentgenol 2004;182(2):473–480.

26. Soderstrom CE, Harms SE, Farrell RS Jr, Pruneda JM, Flamig DP. Detection with MR imaging of residual tumor in the breast soon after surgery. AJR Am J Roentgenol 1997;168(2):485–488.

27. Viehweg P, Heinig A, Lampe D, Buchmann J, Heywang-Köbrunner SH. Retrospective analysis for evaluation of the value of contrast-enhanced MRI in patients treated with breast conservative therapy. MAGMA 1998;7(3):141–152.

28. Krämer S, Schulz-Wendtland R, Hagedorn K, Bautz W, Lang N. Magnetic resonance imaging in the diagnosis of local recurrences in breast cancer. Anticancer Res 1998;18(3C):2159–2161.

29. Jacobs L. Positive margins: the challenge continues for breast surgeons. Ann Surg Oncol 2008;15(5):1271–1272.

30. Krouskop TA, Wheeler TM, Kallel F, Garra BS, Hall T. Elastic moduli of breast and prostate tissues under compression. Ultrason Imaging 1998;20(4):260–274.